JOURNAL OF COMPUTATIONAL PHYSICS 46, 15–38 (1982)

Implicit Time Integration for Plasma Simulation

BRUCE I. COHEN, A. BRUCE LANGDON, AND A. FRIEDMAN

Lawrence Livermore National Laboratory,
University of California, Livermore, California 94550

Received August 24, 1981; revised November 19, 1981

To increase the size of the time step, and thereby extend the applicability of kinetic plasma simulation, analysis of the stability and accuracy of implicit time integration schemes for plasma particle-in-cell simulation and the synthesis of new algorithms have been undertaken. Three classes of implicit algorithms are considered in general form. Stability and accuracy calculations provide guidelines for the design and application of implicit simulation algorithms, as illustrated in the construction of new difference schemes with desirable properties. Of particular interest are the relaxation of stability constraints on the time step, strong damping of unwanted high-frequency modes, accuracy of the simulation of low-frequency phenomena, numerical secular acceleration, and numerical stability of fast and slow space-charge waves. The potency of higher order accurate differencing schemes in reducing undesirable numerical effects is demonstrated.

1. INTRODUCTION

Our goal is to increase the size of the time step in kinetic plasma simulation, in order to extend the applicability to problems of wider physical interest. In this paper, we examine the stability and accuracy of implicit time integration schemes for plasma simulation. We present analyses of three classes of differencing algorithms, and show how to create new schemes with desired properties. Much of the analysis is an extension of that presented by Langdon in an earlier discussion of time integration in particle simulation [1]. In an earlier paper [2], we outlined a simple scheme for direct implicit particle-in-cell simulation, an attractive alternative to the moment-equation method [3, 4]. In another paper [5], we more generally formulate our method for direct implicit simulation, and describe many of its important properties. This analysis of time differencing is applicable to the moment method as well as to our direct method.

The results of our stability and accuracy calculations delineate problem areas and provide guidelines for the design and application of implicit simulation algorithms. Of particular interest are the relaxation of $\omega\Delta t$ stability constraints, strong selective damping of high-frequency modes ($\omega\Delta t \gtrsim 1$), the accuracy of simulation of low-frequency phenomena ($\omega\Delta t \lesssim 1$), numerical secular acceleration, and the numerical stability of fast and slow space-charge waves. We find that most undesirable numerical effects are much diminished in our schemes with damping at third order in

0021-9991/82/040015-24$02.00/0

581/46/1-2

Δt, as compared with lower-order schemes. Our analysis motivates and guides the design of algorithms which retain desirable dissipation of high-frequency oscillations while minimizing unwanted damping of low-frequency oscillations and the concomitant cooling of particles. Here, we shall discuss simulations having only the electrostatic field; similar techniques are applicable to more general physics models.

The paper is organized as follows: A simple-harmonic-oscillator analysis of cold-plasma wave dispersion for three classes of implicit algorithms is presented in Section 2. We establish the essential stability and accuracy properties of low-frequency oscillations, and describe our synthesis of time-differencing schemes with optimal properties. The selective reader should give this section the most attention. The warm-plasma dielectric functions for our implicit algorithms are calculated in Section 3. We synthesize magnetized implicit schemes in Section 4. Section 5 contains a discussion of the numerical cooling and heating of particles in the three classes of algorithms. Section 6 has an outline of future directions we anticipate this research might pursue. A proof of the need for implicit differencing to stabilize time integration when $\omega\Delta t \gg 1$ and a discussion of filtering are given in Appendix A. The numerical stability of fast and slow space-charge waves is assessed in Appendix B.

2. Harmonic-Oscillator Analysis of Cold-Plasma Wave Dispersion

Presented here are the analyses of the stability and accuracy of three classes of implicit algorithms. The results of these calculations lead directly to the synthesis of new schemes with desired properties; examples are presented here. The most important design issues are the relaxation of $\omega\Delta t$ stability constraints, strong damping of high-frequency modes ($\omega\Delta t \gtrsim 1$) and accuracy of the simulation of low-frequency phenomena ($\omega\Delta t \lesssim 1$).

A normal-mode analysis of time-integration schemes with which the temporal stability and accuracy of any algorithm can be determined was presented in [1]. The simplest calculation consists of taking the finite-difference equations, ignoring spatial-grid effects ($k\Delta x \to 0$), and determining how a cold-plasma oscillation is reproduced. For the elementary unmagnetized electrostatic algorithms considered here, the electrons undergo simple harmonic oscillations. Many features of the time integration are learned most directly by applying the difference scheme to a single-particle harmonic oscillator. These calculations can be extended to find linear dispersion properties of warm plasma, with or without finite Δx [1].

It must be kept in mind that stability and dispersion properties built into these time-differencing algorithms are only realized fully when the implicit equations are solved exactly. In practice it may be necessary to iterate. Starting values for the iteration, and the iteration process itself, will need to be chosen with this in mind if a small number (e.g., one!) of iterations is to suffice.

Class C

The first class of algorithms we shall consider was introduced in [1]. It was observed that the linear response of the particle displacement to an acceleration, for a

family of second-order accurate schemes, could be cast in each case into the general form

$$\mathbf{x}_n = (c_0\mathbf{a}_n + c_1\mathbf{a}_{n-1} + \cdots + c_{k-2}\mathbf{a}_{n-k+2})\,\Delta t^2 + \mathbf{x}'_n \tag{1a}$$

$$\mathbf{a}_{n-1} = (\mathbf{x}'_n - 2\mathbf{x}'_{n-1} + \mathbf{x}'_{n-2})/\Delta t^2 \tag{1b}$$

i.e., the position differs from the leapfrog result $\mathbf{x}'$ by an amount involving the acceleration at only a few time steps, with adjustable constants $\{c\}$. Eliminating $\mathbf{x}'$, we obtain

$$\begin{aligned}(\mathbf{x}_n - 2\mathbf{x}_{n-1} + \mathbf{x}_{n-2})/\Delta t^2 = \mathbf{a}_{n-1} &+ c_0(\mathbf{a}_n - 2\mathbf{a}_{n-1} + \mathbf{a}_{n-2}) \\ &+ c_1(\mathbf{a}_{n-1} - 2\mathbf{a}_{n-2} + \mathbf{a}_{n-3}) + \cdots .\end{aligned} \tag{2}$$

With the right sides of Eqs. (1a) and (2) truncated to just the first term in each, we recover the conventional leapfrog scheme. For c_0 finite, the algorithm becomes implicit if $\mathbf{a}_n$ depends on $\mathbf{x}_n$. Additional terms on the right sides of these equations introduce more past information and, as we shall demonstrate, can help control damping.

Difference equations incorporating a velocity can be formulated in many ways: From (1) with $\mathbf{x}'_{n+1} - \mathbf{x}'_n = \mathbf{v}_{n+1/2}\Delta t$,

$$(\mathbf{x}_{n+1} - \mathbf{x}_n)/\Delta t = c_0(\mathbf{a}_{n+1} - \mathbf{a}_n)\,\Delta t + c_1(\mathbf{a}_n - \mathbf{a}_{n-1})\,\Delta t + \cdots + \mathbf{v}_{n+1/2} \tag{3a}$$

$$(\mathbf{v}_{n+1/2} - \mathbf{v}_{n-1/2})/\Delta t = \mathbf{a}_n. \tag{3b}$$

Or, from (2),

$$(\mathbf{x}_{n+1} - \mathbf{x}_n)/\Delta t = \mathbf{v}_{n+1/2} \tag{4}$$

$$\begin{aligned}(\mathbf{v}_{n+1/2} - \mathbf{v}_{n-1/2})/\Delta t = \mathbf{a}_n &+ c_0(\mathbf{a}_{n+1} - 2\mathbf{a}_n + \mathbf{a}_{n-1}) \\ &+ c_1(\mathbf{a}_n - 2\mathbf{a}_{n-1} + \mathbf{a}_{n-2}) + \cdots .\end{aligned}$$

In application, (3) requires less storage of past information.

We now assume that there is harmonic oscillation and introduce the Fourier representation $(\mathbf{x}_n^{(1)}, \mathbf{a}_n^{(1)}) = (\mathbf{X}, \mathbf{A})\,z^n$, where $z \equiv \exp(-i\omega\Delta t)$. Then, from Eq. (1) or (2),

$$X/A\Delta t^2 = c_0 + c_1/z + c_2/z^2 + \cdots + z/(z-1)^2. \tag{5}$$

In a simple harmonic oscillator, the acceleration and particle displacements are related by $\mathbf{A} = -\omega_0^2\mathbf{X}$, with use of which, the following dispersion relation is obtained

$$1/(\omega_0\,\Delta t)^2 + c_0 + c_1/z + c_2/z^2 + \cdots + z/(z-1)^2 = 0. \tag{6}$$

This class of algorithms is described as being second-order accurate inasmuch as for $\omega_0^2 \Delta t^2 \ll 1$ [1],

$$\begin{aligned} \pm \mathrm{Re}\ \omega/\omega_0 &= 1 + \tfrac{1}{2}(\omega_0 \Delta t)^2 \left(\tfrac{1}{12} - c_0 - c_1 - \cdots\right) + \mathcal{O}(\Delta t^3) \\ \mathrm{Im}\ \omega/\omega_0 &= -\tfrac{1}{2}(\omega_0 \Delta t)^3 \left(c_1 + 2c_2 + \cdots\right) + \mathcal{O}(\Delta t^4). \end{aligned} \tag{7}$$

These expressions can be obtained by rewriting Eq. (6) as

$$(1/\omega_0^2 \Delta t^2) + c_0 + c_1 e^{i\theta} + c_2 e^{2i\theta} + \cdots - 1/(4 \sin^2 \theta/2) = 0, \tag{8}$$

where $\theta \equiv \omega \Delta t$, and then linearizing about $\omega \cong \omega_0$.

For general $\omega_0 \Delta t$, we wish to determine conditions on $\{c_0, c_1, \ldots\}$ such that $\mathrm{Im}\ \omega \leqslant 0$, i.e., so that the algorithm is stable. A simple subclass of algorithms for which we now make such a determination is that with $c_s = 0$ for $s \geqslant 2$, whose dispersion relation is

$$c_0' z(z-1)^2 + c_1 (z-1)^2 + z^2 = 0, \tag{9}$$

where $c_0' \equiv c_0 + 1/\omega_0^2 \Delta t^2$. Instability occurs for $c_1 < 0$ or $c_0' < 0$. Oscillations are stable if $c_1 \geqslant 0$ and

$$c_0' \geqslant c_1 + \tfrac{1}{4}. \tag{10}$$

The standard leapfrog stability limit is recovered for $c_0 = c_1 = 0$. The results of solution of Eq. (9) are diagramed in Fig. 1. The stability boundary is plotted in Fig. 1a along with the locus of points corresponding to the most weakly damped normal mode whose damping has been maximized with respect to c_0' (or c_1) for fixed c_1 (or c_0').

It is important to keep in mind that $c_0' \to c_0$ in the limit of very large time step, and that stability then demands nonzero c_0, i.e., implicitness. Very small time step corresponds to large c_0', and the stability condition Eq. (10) is more easily satisfied.

The value of $|z|_{\text{min-max}}$ for the least damped mode, whose damping has been maximized with respect to c_1 or c_0', is plotted as a function of these variables in Fig. 1b, c. Dissipation is introduced with choice of positive c_1. Strong damping of the plasma oscillation is usually desired over a wide range of large time steps. The point $c_0 = 0.302$ and $c_1 = 0.04$, on the $|z|_{\text{min-max}}$ locus of Fig. 1, corresponds to an optimized scheme for which $|z| \sim 0.5$ as $\omega_0 \Delta t \to \infty$. At low frequencies, $\omega_0^2 \Delta t^2 \ll 1$, the oscillations are reproduced accurately, with very weak damping,

$$\pm \mathrm{Re}\ \omega/\omega_0 = 1 - 0.13(\omega_0 \Delta t)^2 + \cdots, \quad \mathrm{Im}\ \omega/\omega_0 = -0.02(\omega_0 \Delta t)^3 + \cdots.$$

We will refer to this choice of c's as the "optimized C_1 scheme."

Denavit [3, 6] has used implicit algorithms that can be cast in terms of Eq. (1). His first particle-pushing difference scheme (J_1) consists of

$$\mathbf{v}_{n+1} - \mathbf{v}_n = (\tfrac{3}{4}\mathbf{a}_{n+1} + \tfrac{1}{4}\mathbf{a}_{n-1}) \Delta t \tag{11a}$$

$$\mathbf{x}_{n+1} - \mathbf{x}_n = (\tfrac{3}{4}\mathbf{v}_{n+1} + \tfrac{1}{4}\mathbf{v}_{n-1}) \Delta t. \tag{11b}$$

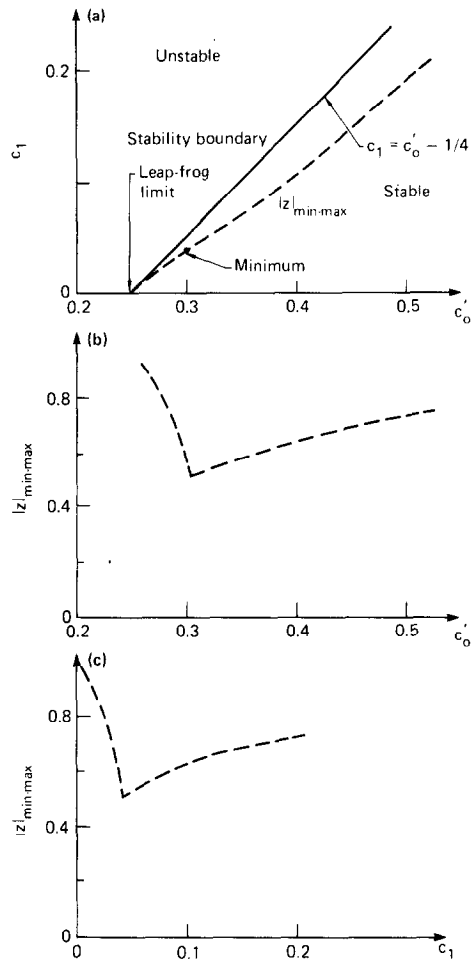

FIG. 1. (a) Stability diagram for difference schemes with $c_0, c_1 \neq 0$ and $c_{s>2} \equiv 0$, $c_0' \equiv c_0 + 1/\omega_0^2 \Delta t^2$. The locus of points along which the maximum value of $|z|$ is minimized, is labeled $|z|_{\text{min-max}}$. The absolute minimum $|z|$ of the most weakly damped normal mode occurs at $c_0 \cong 0.3$, $c_1 \cong 0.04$, and $|z| \cong 0.5$. (b) The $|z|_{\text{min-max}}$ curve minimized with respect to c_1 plotted against c_0'. (c) The $|z|_{\text{min-max}}$ curve minimzed with respect to c_0' plotted against c_1.

For a simple harmonic oscillator of frequency ω_0, Eqs. (11) lead to the dispersion relation

$$\begin{aligned} -1/\omega_0^2 \Delta t^2 = X/A\Delta t^2 &= (3z/4 + 1/4z)^2/(z-1)^2 \\ &= (9/16) + (1/8z) + (1/16z^2) + z/(z-1)^2. \end{aligned} \tag{12}$$

Thus, comparing with Eq. (5), we identify $c_0 = \frac{9}{16}$, $c_1 = \frac{1}{8}$, and $c_2 = \frac{1}{16}$. Equation

(12) is a quartic and has two pairs of stable complex-conjugate solutions for z. For low frequency, $\omega_0^2 \Delta t^2 \ll 1$, there are weakly damped oscillations

$$\pm \mathrm{Re}\ \omega/\omega_0 = 1 - (\omega_0 \Delta t)^2/3 + \cdots, \qquad \mathrm{Im}\ \omega/\omega_0 = -(\omega_0 \Delta t)^3/8 + \cdots,$$

and a pair of heavily damped extraneous modes. At high frequencies, $|z|$ approaches $1/\sqrt{3}$.

Denavit's second scheme (J_2) has increased damping for $\omega_0^2 \Delta t^2 \gg 1$ and smaller damping and frequency shift for $\omega_0^2 \Delta t^2 \ll 1$. It is [3]

$$\mathbf{v}_{n+1} - \mathbf{v}_n = (9\mathbf{a}_{n+1} + 6\mathbf{a}_n + \mathbf{a}_{n-1})\, \Delta t/16 \tag{13}$$

and similarly for $\mathbf{x}_{n+1} - \mathbf{x}_n$. Corresponding coefficients in (1) are $c_0 = 81/256$, $c_1 = 14/256$, and $c_2 = 1/256$. Errors in low-frequency oscillations are

$$\pm \mathrm{Re}\ \omega/\omega_0 = 1 - 7(\omega_0 \Delta t)^2/48 + \cdots, \quad \mathrm{Im}\ \omega/\omega_0 = -(\omega_0 \Delta t)^3/32 + \cdots.$$

At high frequencies, z approaches $-\frac{1}{3}$.

Denavit's schemes have the advantage that $\mathbf{x}$ and $\mathbf{v}$ are defined at the same time levels. They are, however, less accurate at low frequencies and require more storage of past accelerations and velocities than our optimized C_1 scheme.

Class D

A classic second-order stiffly stable scheme for a first-order ordinary differential equation $dy/dt = f$ is [7, 8]

$$(y_{n+1} - y_n)/\Delta t - \tfrac{1}{3}(y_n - y_{n-1})/\Delta t = \tfrac{2}{3} f_{n+1}.$$

Using this for $d\mathbf{x}/dt = \mathbf{v}$ and $d\mathbf{v}/dt = \mathbf{a}$, setting $\mathbf{x}_n = \mathbf{X} z^n$, etc., and eliminating $\mathbf{V}$, we obtain

$$(z-1)^2 (\tfrac{3}{2} - \tfrac{1}{2} z^{-1})^2\, \mathbf{X} = z^2 \mathbf{A} \Delta t^2. \tag{14}$$

The form of this equation motivates consideration of the more general class of schemes for which

$$z^2 \mathbf{A} \Delta t^2 = (z-1)^2\, D(z^{-1})\, \mathbf{X} \tag{15a}$$

$$= (z-1)^2 (d_0 + d_1/z + d_2/z^2 + \cdots)\, \mathbf{X}, \tag{15b}$$

where $D(z^{-1})$ is a polynomial in z^{-1}, such that $D(1) = 1$ and roots of $D(z^{-1}) = 0$ must be inside the unit circle in the complex z plane (i.e., damped). Equation (15b) corresponds to the difference equation

$$\mathbf{a}_{n+1} \Delta t^2 = d_0(\mathbf{x}_{n+1} - 2\mathbf{x}_n + \mathbf{x}_{n-1}) + d_1(\mathbf{x}_n - 2\mathbf{x}_{n-1} + \mathbf{x}_{n-2}) + \cdots. \tag{16}$$

This result is found by expanding (15b) as a polynomial in z, then identifying the time level of each $\mathbf{x}$ term from its power of z. This class of algorithm will now be made second-order accurate, as was class C.

The dispersion relation for a linear oscillator is

$$A\Delta t^2/X = -\omega_0^2 \Delta t^2 = ((z-1)/z)^2(d_0 + d_1/z + d_2/z^2 + \cdots). \tag{17}$$

We find the solution ω for low frequency, $\omega_0^2 \Delta t^2 \ll 1$, by rewriting (17) analogous to (8)

$$((2/\omega_0 \Delta t)\sin(\omega \Delta t/2))^{-2} = e^{i\omega\Delta t} D(e^{i\omega \Delta t}).$$

Now expand in powers of Δt; choose coefficients $\{d_i\}$ so that $D(1) = 1$ (to force $\omega \to \omega_0$ as $\Delta t \to 0$) and to eliminate the term of order Δt. Keeping terms through order Δt^3, this yields

$$\begin{aligned}(\omega_0^2/\omega^2) + \tfrac{1}{3}(\omega_0 \Delta t/2)^2 = 1 &- \tfrac{1}{2}(\omega \Delta t)^2 (d_0 + 4d_1 + 9d_2 + \cdots) \\ &- (i/6)(\omega \Delta t)^3 (d_0 + 8d_1 + 27d_2 + \cdots)\end{aligned}$$

with

$$1 = d_0 + d_1 + d_2 + \cdots, \qquad 0 = d_0 + 2d_1 + 3d_2 + \cdots. \tag{18}$$

From this we find

$$\begin{aligned}\pm \mathrm{Re}\ \omega/\omega_0 &= 1 + \tfrac{1}{4}(\omega_0 \Delta t)^2 (\tfrac{1}{6} + d_0 + 4d_1 + 9d_2 + \cdots) \\ \mathrm{Im}\ \omega/\omega_0 &= \tfrac{1}{12}(\omega_0 \Delta t)^3 (d_0 + 8d_1 + 27d_2 + \cdots).\end{aligned} \tag{19}$$

The other, more damped, modes are given by the zeros of $D(z^{-1})$.

The simplest example of these algorithms has $d_s = 0$ for $s \geqslant 2$; then from (18) we find $d_0 = 2$, $d_1 = -1$. To create corresponding difference equations including a velocity, we can factor Eq. (15b) as

$$\begin{aligned}z^{1/2}\mathbf{V}\Delta t &= \mathbf{X}(z-1) \\ z\mathbf{A}\Delta t &= z^{1/2}\mathbf{V}(1-z^{-1})(2-z^{-1}) = z^{1/2}\mathbf{V}(2 - 3z^{-1} + z^{-2}).\end{aligned}$$

Using the power of z in each term to identify the time level, we find equations that might be used in a code:

$$\mathbf{x}_{n+1} - \mathbf{x}_n = \mathbf{v}_{n+1/2}\Delta t \tag{20a}$$

$$\mathbf{v}_{n+1/2} - \mathbf{v}_{n-1/2} = \tfrac{1}{2}\mathbf{a}_{n+1}\Delta t + \tfrac{1}{2}(\mathbf{v}_{n-1/2} - \mathbf{v}_{n-3/2}). \tag{20b}$$

We shall later refer to this as "scheme D_1."

The dispersion relation becomes

$$(\omega_0 \Delta t)^2 z^3 + (2z-1)(z-1)^2 = 0. \tag{21}$$

This scheme saves $\mathbf{v}_{n-3/2}$ in addition to the $\mathbf{v}_{n-1/2}$ and $\mathbf{x}_n$ saved in a conventional explicit leapfrog algorithm, which leads to the cubic dispersion relation Eq. (21). Denavit's schemes require saving two additional quantities, $\mathbf{v}_{n-1}$ and $\mathbf{a}_{n-1}$ (or recalculating $\mathbf{a}_{n-1}$), and give quartic dispersion relations.

For low frequencies, $\omega_0^2 \Delta t^2 \ll 1$, Eq. (21) describes weakly damped plasma waves with

$$\pm \mathrm{Re}\, \omega/\omega_0 = 1 - (11/24)(\omega_0 \Delta t)^2 + \cdots, \qquad \mathrm{Im}\, \omega/\omega_0 = -(\omega_0 \Delta t)^3/2 + \cdots,$$

and an extraneous damped mode with $|z| \to \frac{1}{2}$. For high frequencies, the modes are much better damped, $|z| \to (\omega_0 \Delta t)^{-2/3}$, than in class C schemes. The reason is that the only acceleration in (16) is $\mathbf{a}_{n+1}$; no earlier $\mathbf{a}$'s are used. In application to plasma simulation, this means that a D scheme attempts to force charge neutrality in one time step, in the limit $\Delta t \to \infty$.

From (19) it is easily seen that we can arrange for damping of order Δt^5 by choosing $d_0 = \frac{5}{2}$, $d_1 = -2$, and $d_2 = \frac{1}{2}$, then verifying that the zeros ($z^{-1} = 2 \pm i$) of $D(z^{-1})$ are damped. We shall later refer to this as "scheme D_2."

First-Order Schemes

It is illuminating to compare the stability and accuracy properties of *first*-order schemes with those of the second-order schemes. A class of such algorithms, used by Mason [4], is equivalent to

$$\begin{aligned} (\mathbf{v}_{n+1/2} - \mathbf{v}_{n-1/2})/\Delta t &= \alpha \mathbf{a}_{n+1} + ((1-\alpha)/4)(\mathbf{a}_{n+1} + 2\mathbf{a}_n + \mathbf{a}_{n-1}) \\ (\mathbf{x}_{n+1} - \mathbf{x}_n)/\Delta t &= \mathbf{v}_{n+1/2}. \end{aligned} \tag{22}$$

These algorithms are implicit and stable for $\alpha \geqslant 0$. Proceeding as before, we obtain the dispersion relation

$$X/A\Delta t^2 = (\alpha z^2 + (1-\alpha)(z+1)^2/4)/(z-1)^2 = -1/\omega_0^2 \Delta t^2. \tag{23}$$

At low frequency, $\omega_0^2 \Delta t^2 \ll 1$,

$$\begin{aligned} \pm \mathrm{Re}\, \omega/\omega_0 &= 1 - [2 + 3\alpha(\alpha+1)](\omega_0 \Delta t)^2/24 + \cdots, \\ \mathrm{Im}\, \omega/\omega_0 &= -\alpha \omega_0 \Delta t/2. \end{aligned}$$

Hence, plasma waves will be damped for $\alpha > 0$, and the attenuation or amplification of a linear mode after time $t = n\Delta t$ is given by $|z^n| = \exp(-\alpha \omega_0^2 t \Delta t/2)$. At low frequencies, $\omega_0^2 \Delta t^2 < 1$, note that the higher order accurate difference schemes are generally much less dissipative than first-order schemes. The damping rates in the higher order schemes scale as a higher power of $\omega_0 \Delta t$, which is usually an advantage in that low-frequency phenomena will be more accurately reproduced.

Solving Eq. (23), a quadratic in z, we find that both normal modes are damped for $\alpha > 0$. For $\omega_0^2 \Delta t^2 \gg 1$ and $0 \leqslant \alpha < 1$,

$$|z| = ((1-\alpha)/(1+3\alpha))^{1/2} \tag{24}$$

which is stable. To increase damping at high frequencies, α must increase. This in turn raises the damping rate at low frequencies, which is proportional to $\alpha\Delta t$. To obtain as much damping at high frequencies as we had in the higher order schemes, the nonphysical damping rate at low frequencies would be far higher in the first-order scheme. A specific example of interest is given by choosing $\alpha = \frac{3}{7}$, which gives $|z| = \frac{1}{2}$ for $\omega_0^2\Delta t^2 \gg 1$, approximately the same asymptotic damping as the optimized C_1 scheme.

Summary of Simple-Harmonic-Oscillator Analysis

The principal conclusions of this subsection are as follows: Relaxation of the $\omega_p\Delta t$ stability constraint in a plasma simulation requires implicitness, as shown here for the C schemes and in general in Appendix A. The coefficients in our difference equations

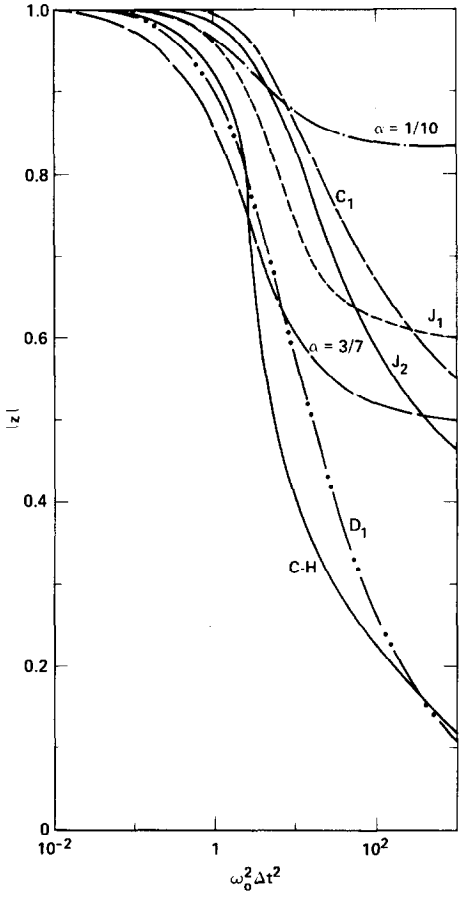

FIG. 2. The absolute value $|z| = |\exp(-i\omega\Delta t)|$ of the least damped simple-harmonic oscillator normal mode versus $\omega_0^2\Delta t^2$ in the J_1 and J_2 schemes of Denavit (Eqs. (11) and (13)), Curtiss and Hirschfelder (C–H, Eq. (14)), first-order schemes (22) with $\alpha = 3/7$ and $1/10$, the optimized C_1 scheme ($c_0 = 0.302$, $c_1 = 0.04$), and the D_1 scheme ($d_0 = 2$, $d_1 = -1$).

that control the degree of implicitness and that govern dissipation jointly determine stability, as illustrated in Eq. (10) and Fig. 1. For $\omega_0^2 \Delta t^2 \gg 1$, implicit schemes may be stable, but the high-frequency oscillations are necessarily distorted; therefore, damping is generally desirable. We have devised several schemes that efficiently damp high-frequency oscillations. These can be compared in Fig. 2 where $|z|$ for the least damped simple-harmonic oscillator normal mode is plotted as a function of $\omega_0^2 \Delta t^2$. These schemes require saving past particle coordinate data. How much past data must be saved depends on the particular scheme, and its minimization should be an important design consideration. Low-frequency oscillations can be simulated with high accuracy. The dissipation rate can be removed to high order in Δt, for $\omega_0 \Delta t < 1$, with proper choice of coefficients $\{c_0, c_1, ...,\}$ in Eq. (1) or (3), or $\{d_0, d_1, ...,\}$ in Eq. (16).

3. Warm Plasma Dispersion

The linear response of a warm plasma is characterized by its dispersion function $\varepsilon(\mathbf{k}, \omega)$. Evaluation of this transcendental function is aided by expressing it as a sum of the dispersion function for the leapfrog integration scheme ε_{lf}, plus a term $\delta\chi$. Methods for evaluation of ε_{lf} are suggested in an appendix to [1]. For class C schemes $\delta\chi$ is simply expressed in terms of the velocity-space Fourier transform of the zero-order velocity-distribution function $f_0(\mathbf{v})$ [1]. Here we shall adapt that derivation to find a similar result for D schemes.

The plasma-density response is due to deflectons of the particle positions from their unperturbed orbits, due to the accelerations experienced. For C schemes. the deflection (1) is separated into a leapfrog term plus the $c_s \mathbf{a}_{n-s}$ terms. Using the methods of [1] leads immediately to[1]

$$\varepsilon(\mathbf{k}, \omega) = \varepsilon_{\text{lf}}(\mathbf{k}, \omega) + \omega_{\text{p}}^2 \Delta t^2 \sum_{s=0}^{k-2} c_s \int d\mathbf{v} f_0(\mathbf{v}) e^{i(\omega - \mathbf{k}\cdot\mathbf{v})s\Delta t}. \tag{25}$$

For D schemes we begin by looking for a result analogous to (1). For leapfrog integration we have, from (5), $\mathbf{X}' = z^{-1}\mathbf{A}\Delta t^2/(1 - z^{-1})^2$. For D schemes, from (15a) we have

$$z^{-1} D(z^{-1})\, \mathbf{X} = \mathbf{X}'. \tag{26}$$

Thus, the difference $\mathbf{X} - \mathbf{X}'$ is given by

$$D(z^{-1})(\mathbf{X} - \mathbf{X}') = z\mathbf{X}' - D(z^{-1})\, \mathbf{X}' \tag{27a}$$

$$= ((1 - z^{-1} D(z^{-1}))/(1 - z^{-1})^2)\, \mathbf{A}\Delta t^2. \tag{27b}$$

The last form appears to be a rational function in z^{-1} but, in fact, it is seen to simply be a polynomal in z^{-1}, once we use the conditions imposed on the form of $D(z^{-1})$.

[1] This expression corrects Eq. (28) of [1], which contains a spurious factor s in the summand.

For accuracy we expect $\mathbf{X}$ to be close to $\mathbf{X}'$ for low-frequency time dependence, i.e., $z^{-1}D(z^{-1}) \cong 1$ for $z^{-1} \cong 1$). The conditions can be expressed as $[1-z^{-1}D(z^{-1})]=0$ at $z^{-1}=1$, for consistency, and $(d/dz^{-1})[1-z^{-1}D(z^{-1})]=0$ at $z^{-1}=1$, for second-order accuracy. These are the same as (18); in the present form they show that the numerator of (27b) has a double zero at $z^{-1}=1$, so it can be divided exactly. Thus,

$$D(z^{-1})(\mathbf{X}-\mathbf{X}') = (1 + r_1 z^{-1} + \cdots + r_{k-3} z^{-(k-3)})\, \mathbf{A}\Delta t^2 \tag{28}$$

for a D scheme whose difference equations are of order k. Identify terms like $\mathbf{A}z^{-s}$ with $\mathbf{a}_{n-s}$, etc., to find the equivalent difference equation

$$\begin{aligned} d_0(\mathbf{x}_n - \mathbf{x}'_n) + d_1(\mathbf{x}_{n-1} - \mathbf{x}'_{n-1}) + \cdots + d_{k-2}(\mathbf{x}_{n-k+2} - \mathbf{x}'_{n-k+2}) \\ = (\mathbf{a}_n + r_1 \mathbf{a}_{n-1} + \cdots + r_{k-3}\mathbf{a}_{n-k+3})\, \Delta t^2. \end{aligned} \tag{29}$$

The right-hand side has only a few terms, but $\mathbf{x}-\mathbf{x}'$ is the result of applying the recursive filter D^{-1} to this finite sum. Therefore, the "memory" of past accelerations does not vanish from $\mathbf{x}-\mathbf{x}'$ after $k-2$ steps, as in (1), but decays (rapidly) according to the zeros of $D(z^{-1})$.

For example, in the D_1 scheme ($k=3$), (27) becomes $(2-z^{-1})(\mathbf{X}-\mathbf{X}') = \mathbf{A}\Delta t^2$. Expanding, we obtain

$$\mathbf{X} = \mathbf{X}' + \tfrac{1}{2}[1 + (2z)^{-1} + (2z)^{-2} + \cdots]\, \mathbf{A}\Delta t^2 \tag{30}$$

for $|z| > \frac{1}{2}$. Following the methods of [1], the dispersion function is

$$\varepsilon(\mathbf{k}, \omega) = \varepsilon_{\mathrm{lf}}(\mathbf{k}, \omega) + \tfrac{1}{2}\omega_p^2 \Delta t^2 \sum_{s=0}^{\infty} 2^{-s} \int d\mathbf{v} f_0(\mathbf{v})\, e^{i(\omega - \mathbf{k}\cdot\mathbf{v})s\Delta t}. \tag{31}$$

Although the last term is not a finite sum, as in (25), the series does converge rapidly, especially when $f_0(\mathbf{v})$ varies smoothly.

For the D_2 scheme, from (27) we find

$$\mathbf{X} - \mathbf{X}' = \frac{2 - z^{-1}}{z^{-2} - 4z^{-1} + 5}\, \mathbf{A}\Delta t^2 = -\frac{1}{2}\left[\frac{1}{z^{-1} - 2 + i} + \frac{1}{z^{-1} - 2 - i}\right] \mathbf{A}\Delta t^2.$$

Results analogous to (30) and (31) can be found by a Taylor-series expansion of the fractions.

4. Magnetized Algorithms

A magnetic field is important in many physical applications. In this section we demonstrate how a magnetic field can be added to implicit particle simulation schemes. In particular, we generalize the class C and D schemes to include a magnetic field in such a way as to (1) reproduce the cyclotron gyration of single

particles in a stable fashion and with no damping for any value of the product of cyclotron frequency ω_c and the time step Δt, and (2) model collective modes (waves) in a numerically stable fashion for any wave frequency and time step, with frequency error $\propto \Delta t^2$ and damping $\propto \Delta t^3$ at low frequency, and with substantial dissipation at high frequency.

Magnetized Class C Schemes

We first consider modification of the class C schemes in the form of Eq. (3) to include a magnetic field **B**. Only (3b) changes, becoming

$$(\mathbf{v}_{n+1/2} - \mathbf{v}_{n-1/2})/\Delta t = \mathbf{a}_n + \tfrac{1}{2}(\mathbf{v}_{n+1/2} + \mathbf{v}_{n-1/2}) \times (q\mathbf{B}/mc), \tag{32}$$

where $\mathbf{a}_n$ is due only to an electric field. Eq. (32) is the same as in the usual explicit leapfrog algorithm with centered implicit $\mathbf{v} \times \mathbf{B}$ rotation [9].

We now specialize this model to that commonly used for simulations of Bernstein modes [10] and upper-hybrid waves propagating perpendicularly to **B**. The linear-dispersion relation for long wavelength, upper-hybrid oscillations, is derived by taking $\mathbf{B} = B_0 \hat{\mathbf{z}}$, and by taking $\mathbf{a}_n$ to be $-\omega_p^2 x_n \hat{\mathbf{x}}$, due to electrostatic fields with wave spatial variations in x only. Introducing the Fourier representation for time dependence as in Section 2, we find

$$\begin{aligned} X/A\Delta t^2 = -1/\omega_p^2 \Delta t^2 &= c_0 + c_1/z + c_2/z^2 \\ &\quad + \cdots + z/((z-1)^2 + (z+1)^2\, \omega_c^2 \Delta t^2/4), \end{aligned} \tag{33}$$

where $\omega_c \equiv qB/mc$ is the cyclotron frequency. With no electric field, and, thus, no collective effects ($\omega_p \to 0$), undamped cyclotron gyration is recovered and is described by the solutions of

$$(z-1)^2 + (z+1)^2\, \omega_c^2 \Delta t^2/4 = 0 \tag{34a}$$

viz.,

$$\tan^2 \omega \Delta t/2 = \omega_c^2 \Delta t^2/4. \tag{34b}$$

This modified class C algorithm remains second-order accurate; for $(\omega_c^2 + \omega_p^2)\Delta t^2 \ll 1$, (33) has solutions

$$\begin{aligned} \pm \mathrm{Re}\, \omega/\omega_h &= 1 + \tfrac{1}{2}(\omega_h \Delta t)^2 \left[\tfrac{1}{12} - (\omega_c/2\omega_p)^2 - (c_0 + c_1 + \cdots)(\omega_p/\omega_h)^4\right] \\ &\quad + \mathcal{O}(\Delta t^3) \\ \mathrm{Im}\, \omega/\omega_h &= -\tfrac{1}{2}(\omega_p/\omega_h)(\omega_p \Delta t)^3\, (c_1 + 2c_2 + \cdots) + \mathcal{O}(\Delta t^4), \end{aligned}$$

where ω_h is the hybrid frequency, $\omega_h^2 \equiv \omega_p^2 + \omega_c^2$. For $\omega_c^2 \Delta t^2 \gg 1$ and $\omega_p^2 \Delta t^2 \gg 1$, there are solutions given approximately by

$$c_0 + c_1/z + c_2/z^2 + \cdots = 0.$$

Stability of these solutions ($|z| < 1$) constrains the values of $\{c_i\}$. The remaining two solutions of (33) correspond to modified cyclotron oscillations, whose real frequency has approached $\pm\pi/\Delta t$ (i.e., $z \cong -1$), and whose stability requires

$$c_0 - c_1 + c_2 - \cdots > \tfrac{1}{4}.$$

This necessary, but not sufficient, condition is compatible with (10).

Magnetized Class D *Schemes*

We next introduce **B** into the D schemes in the form of (20):

$$\mathbf{a}_{n+1} = d_0[(\mathbf{v}_{n+1/2} - \mathbf{v}_{n-1/2})/\Delta t - \tfrac{1}{2}(\mathbf{v}_{n+1/2} + \mathbf{v}_{n-1/2}) \times (q\mathbf{B}/mc)] + d_1[(\mathbf{v}_{n-1/2} - \mathbf{v}_{n-3/2})/\Delta t - \tfrac{1}{2}(\mathbf{v}_{n-1/2} + \mathbf{v}_{n-3/2}) \times (q\mathbf{B}/mc)] + \cdots . \quad (35)$$

Single-particle cyclotron gyration is neither damped nor destabilized.

The dispersion relation for long-wavelength, upper-hybrid oscillations, as supported by this difference scheme, is

$$\frac{\Delta\Delta t^2}{\quad} \quad \left[\frac{(z-1)^2}{\quad} \quad \frac{(z+1)^2}{\quad} \quad \omega_c^2\Delta t^2\right]$$

$$\times (d_0 + d_1/z + d_2/z^2 + \cdots). \quad (36)$$

With no electric field and no collective effects ($\omega_p \to 0$), undamped cyclotron oscillations are recovered exactly as in Eq. (34). There are still the extraneous modes given by $D(z^{-1}) = 0$ and discussed in Section 2.

With values of $\{d_i\}$ chosen according to the same constraints (18) as in the unmagnetized case, second-order accuracy is obtained for $\omega_h^2\Delta t^2 \ll 1$,

$$\pm \mathrm{Re}\ \omega/\omega_h = 1 + \tfrac{1}{4}(\omega_h\Delta t)^2 [\tfrac{1}{6} - \tfrac{1}{2}(\omega_c/\omega_h)^2 + (\omega_p/\omega_h)^2 (d_0 + 4d_1 + 9d_2 + \cdots)] + \mathcal{O}(\Delta t^3)$$

$$\mathrm{Im}\ \omega/\omega_h = \tfrac{1}{12}(\omega_p/\omega_h)^2 (\omega_h\Delta t)^3 (d_0 + 8d_1 + 27d_2 + \cdots) + \mathcal{O}(\Delta t^4). \quad (37)$$

In this limit, the upper-hybrid waves are damped $\propto\Delta t^3$ for scheme D_1 and $\propto\Delta t^5$ for scheme D_2.

For $\omega_c^2\Delta t^2 \gg 1$ and $\omega_p^2\Delta t^2 \gg 1$, dispersion relation (36) is well approximated by

$$z^2 + (\omega_c/\omega_p)^2 (z+1)^2 (d_0 + d_1/z + d_2/z^2 + \cdots) = 0. \quad (38)$$

For the D_1 scheme, (38) becomes a cubic. The dissipation of the two oscillatory solutions increases with increasing ω_p/ω_c, as these modes convert from undamped cyclotron gyration to strongly damped Langmuir waves. The remaining mode is damped for any value of ω_c/ω_p. In general, the conditions for damped modes, using both (37) and (38), constrain the acceptable values for $\{d_i\}$.

Remarks

For moderate values of $\omega_c \Delta t$, i.e., $\lesssim 2$, it has usually been desirable that the radius of cyclotron gyration be maintained by the difference scheme; we have preserved this feature. With $\omega_c \Delta t \gg 1$, however, it is not clear what is gained by this. The particle cannot correctly sample the variation of the field across the gyroradius, and noise at frequencies $\gtrsim \Delta t^{-1}$ may artificially *increase* the gyroradius. A scheme which reproduced the $c\mathbf{E} \times \mathbf{B}/B^2$ drift, while causing the gyroradius to decay when $\omega_c \Delta t \gg 1$, might be preferable for a species intended to remain cold; the concomitant cooling of a warm species might be undesirable. These points require further thought.

5. Numerical Cooling and Heating

Another important aspect of numerical accuracy is illuminated by a calculation of the trajectory of a particle drifting through a sinusoidally varying force field, as reproduced by finite-difference equations. Unphysical modifications are introduced by finite time-step effects that depend on wavelength, time step, and particle velocity. (Again we ignore spatial-grid effects, $k\Delta x \to 0$.)

Secular Acceleration

We consider difference algorithms which can be put into the form

$$\begin{aligned} x_{n+1} - x_n &= v_*(v_{n+1/2}, v_{n-1/2}, \ldots)\, \Delta t \\ v_{n+1/2} - v_{n-1/2} &= a_*(a_{n+1}, a_n, \ldots; v_{n-1/2}, v_{n-3/2}, \ldots)\, \Delta t. \end{aligned} \tag{39}$$

and a drifting particle in the wave frame of a small-amplitude sinusoidal electrostatic wave. The unperturbed particle velocity is $v^{(0)}$ and the acceleration field is represented as $a = \tilde{a} \exp(ikx) + \text{c.c.}$ The particle is untrapped, i.e., $|q\phi| \equiv |ma/k| \ll mv^2/2$, and ought to interact adiabatically with the wave. Depending on the functional dependence of v_* and a_*, however, a drifting particle will experience a spurious time-averaged force and will accelerate.

For a small-amplitude wave field, we do a Taylor series expansion of x, v, and a_* in powers of $\tilde{a}$. Then

$$e^{ikx} = \exp[ik(x^{(0)} + v^{(0)} t_n + x^{(1)} + \cdots)].$$

The time-averaged first-order acceleration is zero, and the averaged second-order acceleration in the fixed-wave field is given by

$$\begin{aligned} \langle a_*^{(2)} \rangle &= \langle x^{(1)} \frac{\partial}{\partial x} a_*(x^{(0)}) \rangle \\ &= \langle -ikx^{(1)} \tilde{a}^* \exp(-ikx^{(0)}) + \text{c.c.} \rangle \\ &= -ik\tilde{x}\tilde{a}^* + \text{c.c.} = 2k\, \text{Im}(\tilde{x}\tilde{a}^*), \end{aligned} \tag{40}$$

where $x^{(1)} = \tilde{x}\exp(ikx^{(0)}) + \text{c.c.}$ and we have redefined $x^{(0)}$ as the sum of the former $x^{(0)}$ and $v^{(0)}t$. Equation (40) can be rewritten as

$$\langle a_*^{(2)}\rangle = 2k|\tilde{a}|^2\,\Delta t^2\,\mathrm{Im}(\tilde{x}/\tilde{a}\Delta t^2) = |\tilde{a}|(\omega_{\mathrm{tr}}\Delta t)^2\,\mathrm{Im}(\tilde{x}/\tilde{a}\Delta t^2), \tag{41}$$

where $\omega_{\mathrm{tr}} \equiv |2k\tilde{a}|^{1/2}$ is the trapping frequency, and $\mathrm{Im}(\tilde{x}/\tilde{a}\Delta t^2)$ will be a function of $kv^{(0)}\Delta t$ whose form depends on the difference scheme. In this form for the drag, we see that $(\omega_{\mathrm{tr}}\Delta t)^2$ is a measure of the ratio of the magnitudes of the nonphysical secular acceleration to the physical acceleration induced by the wave field.

The time-averaged power is given by

$$\langle P\rangle = \langle P^{(0)} + P^{(1)} + P^{(2)} + \cdots\rangle = mv^{(0)}\langle(v_{n+1/2} - v_{n-1/2})/\Delta t\rangle^{(2)}$$
$$+ m\langle((v_{n+1/2} + v_{n-1/2})^{(1)}/2)((v_{n+1/2} - v_{n-1/2})^{(1)}/\Delta t)\rangle.$$

The second term on the right side averages to zero, leaving

$$\langle P\rangle \cong \langle P^{(2)}\rangle = mv^{(0)}\langle a_*^{(2)}\rangle, \tag{42}$$

which we recognize as just the product of the zero-order drift velocity and the averaged second-order force.

Class C

For the class of algorithms represented by difference equations (1) or (2), the first-order particle displacement is related to the acceleration by

$$\tilde{x}/\tilde{a}\Delta t^2 = -(4\sin^2(\Theta/2))^{-1} + c_0 + c_1 e^{-i\Theta} + c_2 e^{-2i\Theta} + \cdots, \tag{43}$$

which follows directly from Eq. (5) with $z = \exp(i\Theta)$, where $\Theta \equiv kv^{(0)}\Delta t$. The averaged second-order acceleration is given by

$$\langle a_*^{(2)}\rangle/|\tilde{a}| = -(\omega_{\mathrm{tr}}\Delta t)^2\,(c_1\sin\Theta + c_2\sin 2\Theta + \cdots). \tag{44}$$

The acceleration is bounded, and vanishes at $kv^{(0)}\Delta t = N\pi$, for $N = 0, \pm 1, \pm 2, \ldots$. Particles are accelerated toward the nearest value of $kv^{(0)}\Delta t = 2\pi N$. For $|kv^{(0)}\Delta t| \ll 1$, there is a weak drag force,

$$\langle a_*^{(2)}\rangle/|\tilde{a}| \cong -(kv^{(0)}\Delta t)(\omega_{\mathrm{tr}}\Delta t)^2\,(c_1 + 2c_2 + \cdots).$$

Note the similar dependence on $\{c_n\}$ of the drag and the damping of the simple-harmonic oscillator for $\omega_0\Delta t \ll 1$ in Eq. (7). We can also write this as

$$\langle a_*^{(2)}\rangle\,\Delta t/v^{(0)} = -\tfrac{1}{2}(\omega_{\mathrm{tr}}\Delta t)^4\,(c_1 + 2c_2 + \cdots)$$

which shows the velocity-decay rate depends only on $\omega_{\mathrm{tr}}\Delta t$.

In the optimized C_1 scheme ($c_0 = 0.302$, $c_1 = 0.04$) we find

$$\langle a_*^{(2)} \rangle / |\tilde{a}| = -0.04(\omega_{tr} \Delta t)^2 \sin \Theta. \tag{45}$$

In Denavit's J_1 scheme ($c_0 = \frac{9}{16}$, $c_1 = \frac{1}{8}$, and $c_2 = \frac{1}{16}$), described by difference equations (11), $\tilde{x}$ is related to $\tilde{a}$ according to Eq. (12),

$$\tilde{x}/\tilde{a}\Delta t^2 = -(4 \sin^2(\Theta/2))^{-1} + \tfrac{9}{16} + \tfrac{1}{8} e^{-i\Theta} + \tfrac{1}{16} e^{-2i\Theta}. \tag{46}$$

From Eqs. (41) and (46) we determine that

$$\langle a_*^{(2)} \rangle / |\tilde{a}| = -\tfrac{1}{8}(\omega_{tr} \Delta t)^2 \sin \Theta (1 + \cos \Theta).$$

This is qualitatively similar to the earlier result Eq. (45), but $\langle a_*^{(2)} \rangle$ is slightly skewed so that the slope of the $\langle a_*^{(2)} \rangle$ versus $kv^{(0)}\Delta t$ curve is steeper near $kv^{(0)}\Delta t = 0$ and integer multiples of 2π. We find the bound $|\langle a_*^{(2)} \rangle| \leqslant 0.16(\omega_{tr} \Delta t)^2 |\tilde{a}|$ occurring at $kv^{(0)}\Delta t = \pi/3$ for Denavit's J_1 scheme, as compared to the optimized C_1 scheme for which $|\langle a_*^{(2)} \rangle| \leqslant 0.04(\omega_{tr} \Delta t)^2 |\tilde{a}|$ occurring at $kv^{(0)}\Delta t = \pi/2$. For $|kv^{(0)}\Delta t| \ll 1$, the particles drag to lower speeds,

$$\langle a_*^{(2)} \rangle / |\tilde{a}| \cong -\tfrac{1}{4}(kv^{(0)}\Delta t)(\omega_{tr} \Delta t)^2.$$

The drag on slow particles in Denavit's J_1 scheme, proportional to $c_1 + 2c_2 = 0.25$, is more than 6 times as large as in the optimized C_1 scheme, where $c_1 = 0.04$ and $c_2 = 0$.

In Denavit's later scheme J_2 [3],

$$\langle a_*^{(2)} \rangle / |\tilde{a}| = -\tfrac{7}{128}(\omega_{tr} \Delta t)^2 \sin \Theta (1 + \tfrac{1}{7} \cos \Theta)$$

with a bound $|\langle a_*^{(2)} \rangle| \leqslant 0.055(\omega_{tr} \Delta t)^2 |\tilde{a}|$ occurring at $kv^{(0)}\Delta t = 1.433$. This is one third as large as the bound for Denavit's earlier J_1 scheme but is still larger than the maximum drag in our optimized C_1 scheme. For $|kv^{(0)}\Delta t| \ll 1$, the drag

$$\langle a_*^{(2)} \rangle / |\tilde{a}| \cong -\tfrac{1}{16}(kv^{(0)}\Delta t)(\omega_{tr} \Delta t)^2$$

is four times smaller than in scheme J_1 and 50% larger than in the optimized C_1 scheme.

Class D

The difference algorithm D_1 described earlier in Eq. (20) has properties similar to Denavit's scheme. The linear displacement is related to the acceleration by

$$\tilde{x} = -(\tilde{a}\Delta t^2/4 \sin^2(\Theta/2)) e^{2i\Theta}/(2e^{i\Theta} - 1). \tag{47}$$

Using Eqs. (41) and (47), we calculate that

$$\langle a_*^{(2)} \rangle / |\tilde{a}| = -(\omega_{tr} \Delta t)^2 \sin \Theta / (5 - 4 \cos \Theta).$$

This result is qualitatively like that of the optimized C_1 scheme, but $\langle a_*^{(2)} \rangle$ is skewed to steeper slopes for $kv^{(0)}\Delta t$ equal to even multiples of π, as is Denavit's scheme. For low speeds, $|kv^{(0)}\Delta t| \ll 1$, the particles again drag to lower speeds,

$$\langle a_*^{(2)} \rangle / |\tilde{a}| \cong -(kv^{(0)}\Delta t)(\omega_{tr}\Delta t)^2$$

with scaling the same as the other algorithms but with magnitude four times larger than in Denavit's scheme and 25 times that of the optimized C_1 scheme. The drag is bounded by $|\langle a_*^{(2)} \rangle| \leqslant (\omega_{tr}\Delta t)^2 |\tilde{a}|/3$ occurring at $kv^{(0)}\Delta t = 0.64$, which is about twice the bound on the drag in Denavit's scheme.

First-Order Schemes

For the first-order difference scheme, Eq. (22), the linear displacement $\tilde{x}$ in a sinusoidal force field has been calculated in Eq. (23),

$$\tilde{x} = -(\tilde{a}\Delta t^2/4 \sin^2(\Theta/2))[\alpha e^{i\Theta} + (1-\alpha)\cos^2(\Theta/2)]. \tag{48}$$

We calculate the average acceleration from Eqs. (41) and (48),

$$\langle a_*^{(2)} \rangle / |\tilde{a}| = -\tfrac{1}{2}\alpha(\omega_{tr}\Delta t)^2 \cot(\Theta/2). \tag{49}$$

The acceleration given by Eq. (49) is plotted in Fig. 3. Particles are again accelerated

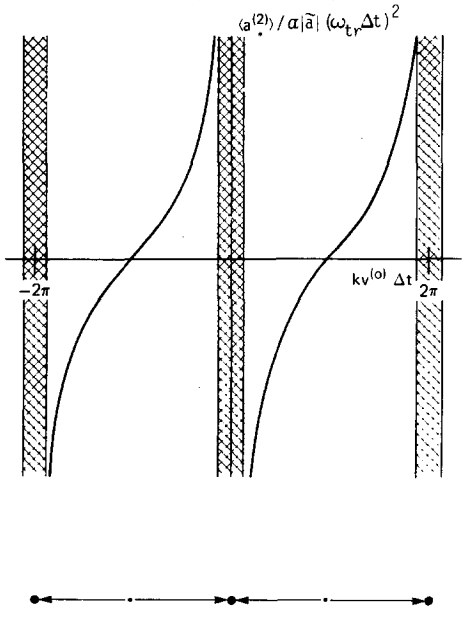

FIG. 3. The average second-order acceleration $\langle a_*^{(2)} \rangle / \alpha |\tilde{a}| (\omega_{tr}\Delta t)^2 = -\cot(kv^{(0)}\Delta t/2)/2$ is plotted against $kv^{(0)}\Delta t$ for a first-order accurate difference scheme. The shaded bands indicate where trapping invalidates the perturbation theory.

toward values of $kv^{(0)}\Delta t$ equal to integer multiples of 2π, where the acceleration appears to become singular. In fact, trapping occurs here, and our perturbation theory then becomes invalid. We determine a quantitative estimate on the regime of validity by setting $|kx^{(1)}| = 1$, at which point our expansion of $\exp(ikx^{(1)})$ fails in the derivation of Eq. (41). The region near $kv^{(0)}\Delta t = 2\pi N$, where trapping occurs, is described by

$$|kx^{(1)}| \cong |2k\tilde{a}|\Delta t^2/(kv^{(0)}\Delta t - 2\pi N)^2 \gtrsim 1. \tag{50}$$

Using $k^2 v_{tr}^2 \equiv \omega_{tr}^2 = |2k\tilde{a}|$, we find that condition equation (50) is equivalent to

$$|v^{(0)} - 2\pi N/k\Delta t| \lesssim v_{tr}$$

which defines the regions of trapped particles.

For $|kv^{(0)}\Delta t| \ll 1$, the particle acceleration is proportional to $\Delta t/kv^{(0)}$,

$$\langle a_*^{(2)} \rangle / |\tilde{a}| \cong -\alpha(\omega_{tr}\Delta t)^2/(kv^{(0)}\Delta t)$$

and *increases* in magnitude as the particle slows down. The acceleration for the first-order scheme is larger by $\mathcal{O}(kv^{(0)}\Delta t)^{-2}$ in the limit of small $|kv^{(0)}\Delta t|$ than that for the second-order schemes described earlier. The maximum acceleration occurs at the onset of trapping, and is $\mathcal{O}(\alpha|\tilde{a}|\omega_{tr}\Delta t)$.

Summary of Numerical Cooling and Heating

The unphysical acceleration (drag) rates for the second-order schemes are all proportional to Δt^3 for slow particles. This scaling and detailed dependence on the difference schemes correspond directly to those for the dissipation rates we found for low-frequency simple harmonic oscillations. Thus, the same mechanism causing damping of low-frequency modes is also responsible for artificial cooling or heating of the plasma as it interacts with electric-field structures. Use of higher order schemes reduces both effects. The absolute cooling or heating rates we obtain depend on the

In contrast, the plasma cooling/heating rates for the first-order schemes are generally much larger than those for the second-order accurate schemes, which argues strongly for the use of the higher order algorithms. Drag rates of first- and second-order schemes can be compared in Fig. 4 where we plot the normalized accelerations $-\langle a_*^{(2)} \rangle / |\tilde{a}|(\omega_{tr}\Delta t)^2 = -\mathrm{Im}(\tilde{x}/\tilde{a}\Delta t^2)$, which are functions only of $kv^{(0)}\Delta t$. Mason [4] has observed numerical cooling of warm plasmas in simulations with a first-order dissipative implicit algorithm. Significantly reduced cooling rates can be achieved by using the higher order accurate integration schemes.

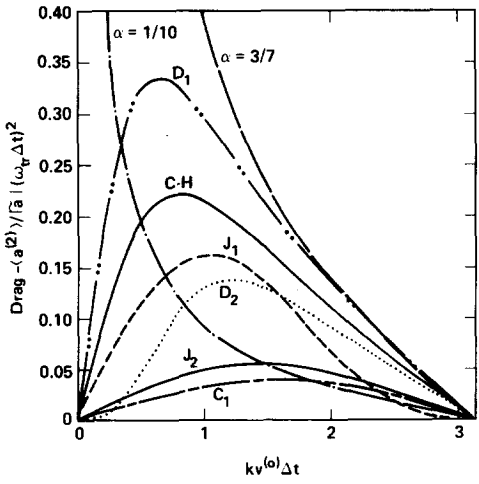

FIG. 4. The normalized drag $-\langle a_*^{(2)}\rangle/|\tilde{a}|(\omega_{tr}\Delta t)^2 = -\mathrm{Im}(\tilde{x}/\tilde{a}\Delta t^2)$ versus $kv^{(0)}\Delta t$ for the J_1 and J_2 schemes of Denavit (Eqs. (11) and (13)), Curtiss and Hirschfelder (C–H, Eq. (14)), first-order schemes (22) with $\alpha = 3/7$ and $1/10$, the optimized C_1 scheme ($c_0 = 0.302$, $c_1 = 0.04$), the D_1 scheme ($d_0 = 2$, $d_1 = -1$), and the D_2 scheme ($d_0 = 5/2$, $d_1 = -2$, $d_2 = 1/2$). The drag has odd symmetry and is periodic with respect to $kv^{(0)}\Delta t$ with period 2π.

6. FUTURE DIRECTIONS

This article presents the design and synthesis of new implicit algorithms for electrostatic particle simulation. Our goal has been to extend the applicability of particle simulation to plasma physics problems in which very large time steps are desirable, if not essential. In so doing, however, we have demanded numerical stability at large Δt, accurate reproduction of low-frequency oscillations, and significant damping of high-frequency modes that are severely distorted by the differencing scheme in any case. Our analyses of stability, accuracy, collective response, and numerical secular acceleration provide important guidelines for the design and optimization of new algorithms, which we have illustrated in the class C and D schemes.

There are numerous areas in which this work should be extended. Our analysis of stability and dispersion properties is strictly applicable only when the implicit difference equations are solved exactly; this analysis should also be applied to the approximate solutions of the implicit difference equations that so far have been implemented [2–4], and to the iterative refinement of those solutions [5]. The effects of a finite spatial grid and spatial-aliasing instabilities [3] should be analyzed. We would like to relax Δt constraints imposed by $kv\Delta t \lesssim 1$ and $\omega_{tr}\Delta t \lesssim 1$. Direct implicit particle-in-cell algorithms suitable for fully electromagnetic physics models should be designed, requiring both implicit time differencing of Maxwell's equations and a relativistic generalization of the particle mover. Finally, we anticipate that, with

experience acquired in physics applications with implicit algorithms, other important issues will emerge to motivate further development and refinement of these algorithms.

APPENDIX A: STABILITY, IMPLICITNESS, AND FILTERING

It is commonly understood that implicit time differencing is required for stable integration of "stiff" systems of differential equations [7, 8]. On the other hand, it has often been tempting to introduce a low-pass filter, into either the particle integration or the field solver, in order to eliminate high frequencies from the simulation without the inconvenience of an implicit equation of motion. We shall show, however, that:

(1) Stable schemes need not include any attenuation of high frequencies, but must be implicit.

(2) Low-pass filtering may in fact *de*stabilize the simulation, even at low frequencies, because of phase errors introduced by the filter.

(3) Filtering considerations *do* enter into design of algorithms with particular accuracy requirements.

Let us regard particle integration as two operations: a filter is applied to the sequence $\{\mathbf{a}_{n+1}, \mathbf{a}_n, \mathbf{a}_{n-1},\ldots,\}$ to produce $\mathbf{a}'_n$, followed by a double time integration of $\{\mathbf{a}'_n, \mathbf{a}'_{n-1},\ldots,\}$ to produce $\mathbf{x}_{n+1}$. Without loss of generality, we assume the use of the centered leapfrog scheme for this integration, whose transfer function is $\mathbf{X}/\mathbf{A}' = z\Delta t^2/(z-1)^2$, which has no phase error for sinusoidal input.

Let us consider the effect of low-pass filtering in an explicit scheme, i.e., one using only $\{\mathbf{a}_n, \mathbf{a}_{n-1},\ldots,\}$, and not $\mathbf{a}_{n+1}$, to produce $\mathbf{a}'_n$ and, thence $\mathbf{x}_{n+1}$. A low-pass filter will introduce a time delay, so that for low frequencies $\mathbf{a}'$ lags behind $\mathbf{a}$ by a time $\tau > 0$. The consequence of this phase error in a feedback loop can be inferred at low frequencies from its effect on a simple harmonic oscillator with continuous time dependence:

$$d^2\mathbf{x}(t)/dt^2 = \mathbf{a}'(t) \cong \mathbf{a}(t-\tau) = -\omega_0^2\mathbf{x}(t-\tau)$$
$$\cong -\omega_0^2[\mathbf{x}(t) - \tau\, d\mathbf{x}(t)/dt].$$

The delay produces an instability with growth rate $\cong\omega_0^2\tau/2$. By including $\mathbf{a}_{n+1}$ in the difference equation, this destabilizing phase error can be reversed.

Now consider two stable implicit schemes, Denavit's (11) and Mason's (22), for which the filter transfer functions are $\mathbf{A}'/\mathbf{A} = z(\frac{3}{4} + \frac{1}{4}z^2)^2$ and $\alpha z + (1-\alpha)(z + 2 + z^{-1})/4$, respectively. The attenuation (modulus of transfer function) by Denavit's filter increases as $|\omega\Delta t|$ rises from 0, but at the Nyquist frequency $\omega = \pi/\Delta t$ (i.e., at $z = -1$) there is *no* attenuation, the modulus is unity. This scheme achieves large time-step stability *without attenuation* at the high frequencies, where instability usually appears with other schemes. Similiarly, Mason's scheme provides strongest

damping of high-frequency modes when $\alpha = 1$ is chosen, for which the filter provides *no* attenuation of high frequencies (Eq. (24)). Conversely, the choice $\alpha = 0$ provides strong low-pass filtering but no damping of high-frequency modes.

For the class of integration methods discussed here, we now show that, in general, an implicit difference equation of motion is required for stability at large $\omega_p^2 \Delta t^2$. It is sufficient to show this for long wavelength, $\gg \lambda_D$, where the electron motion reduces to simple harmonic oscillation. As mentioned before, in an unmagnetized electrostatic simulation the essential particle variables are $\mathbf{x}$ and $\mathbf{a}$; $\mathbf{v}$ is an auxiliary variable. Upon elimination of $\mathbf{v}$, an order-k difference equation of motion can be written as

$$\mathbf{x}_n + \alpha_1 \mathbf{x}_{n-1} + \cdots + \alpha_k \mathbf{x}_{n-k} = \Delta t^2 (\beta_0 \mathbf{a}_n + \beta_1 \mathbf{a}_{n-1} + \cdots + \beta_k \mathbf{a}_{n-k}), \tag{A.1}$$

where either $\alpha_k \neq 0$ or $\beta_k \neq 0$, and $\beta_0 \neq 0$ for an implicit scheme. Again setting $\mathbf{a}_n = -\omega_0^2 \mathbf{x}_n$, then $\mathbf{x}_n = \mathbf{X} z^n$, and we obtain a dispersion relation

$$0 = P(z) \equiv \left(\frac{1}{\omega_0^2 \Delta t^2} + \beta_0 \right) z^k + \left(\frac{\alpha_1}{\omega_0^2 \Delta t^2} + \beta_1 \right) z^{k-1} + \cdots + \left(\frac{\alpha_k}{\omega_0^2 \Delta t^2} + \beta_k \right). \tag{A.2}$$

As $\omega_0^2 \Delta t^2 \to \infty$, the zeros of polynomial $P(z)$ approach those of

$$\beta_0 z^k + \beta_1 z^{k-1} + \cdots \beta_k \tag{A.3}$$

unless $\beta_0 = 0$, i.e., the scheme is not implicit but is explicit, in which case (A.3) is missing some of the zeros of P. For an implicit scheme there is the possibility of stability (all zeros z of (A.2) inside the unit circle for all values of $\omega_0^2 \Delta t^2$).

For an explicit scheme, $\beta_0 = 0$, the polynomial (A.3) has only $k - 1$ (or fewer) roots. Choose a circle in the complex z plane, centered at $z = 0$, with any radius > 1 which encloses these roots. We now show that remaining roots of the dispersion relation lie outside this circle, for sufficiently large $\omega_0^2 \Delta t^2$. Map the circle through the function $P(z)$, as in a Nyquist stability analysis; this will loop around the origin $P = 0$ only $k - 1$ (or fewer) times for sufficiently large $\omega_0^2 \Delta t^2$. Thus, the circle in the z plane does *not* enclose all zeros of P. Since this circle can be chosen arbitrarily large, we know that one (or more) roots diverge, $|z| \to \infty$, as $\omega_0^2 \Delta t^2 \to \infty$.

We have seen that large time-step stability is not a matter of attenuation of high frequencies, but depends strongly on phase characteristics. However, it should be evident that achieving higher accuracy in stable schemes can be regarded as a problem in filter design. For example, choosing polynomial $D \equiv 1$ in (15a) produces a stable first-order scheme (the same as (22) with $\alpha = 1$); but we tailor $D(z^{-1})$ in order to obtain higher accuracy of low and moderate frequencies without introducing offensive new modes.

APPENDIX B: STABILITY OF FAST AND SLOW SPACE-CHARGE WAVES

The simple-harmonic-oscillator stability analysis in Section 2 is applicable to a cold, uniform, nondrifting plasma. With the addition of a drift, u_0, the plasma waves at frequencies $\omega = \pm\omega_p$ are Doppler-shifted to $\omega = ku_0 \pm \omega_p$, where the higher (lower) frequency wave is termed the fast (slow) space-charge wave. In the presence of a resistive background the fast wave damps and the slow wave can be destabilized if $ku_0 > \omega_p$. This is the underlying physical mechanism for the resistive-wall amplifier [11]. We address here whether implicitness and frequency-dependent dissipation in difference equations will artificially destabilize either space-charge wave. We find that the numerical stability of these waves is unaffected if the dissipation is introduced in a Galilean-invariant manner.

We first consider the differencing scheme Eq. (2) The impact of including a plasma drift on the linear stability analysis given in Eqs. (5)–(10) is simply to introduce a Doppler shift in the mode frequency

$$z \equiv e^{-i\omega\Delta t} \to z \equiv \exp(-i\omega\Delta t + iku_0\Delta t).$$

The form and conclusions of Eqs. (5)–(10) are unchanged. Thus, the damping and stability considerations are the same as for the simple harmonic oscillator, and both fast and slow waves are stable if $c_1 \geqslant 0$ and

$$c_0 + 1/\omega_p^2\Delta t^2 \geqslant c_1 + \tfrac{1}{4}.$$

Equation (9) is equivalent to

$$\sin^2(\theta/2) = (\omega_p\Delta t/2)^2\,[1 - 4c_0\sin^2(\theta/2) - 4c_1\sin^2(\theta/2)\,e^{i\theta}], \tag{B.1}$$

where $\theta \equiv \omega\Delta t - ku_0\Delta t$. In the limit $\omega_p\Delta t \ll 1$, the solutions of Eq. (B.1) are

$$\omega = ku_0 \pm \omega_p(1 - c_0\omega_p^2\Delta t^2/2 \mp ic_1\omega_p^3\Delta t^3/2), \tag{B.2}$$

which explicitly exhibits damping proportional to $(\omega_p\Delta t)^3$ of *both* fast and slow waves if $c_1 > 0$.

Changing the time centering of Poisson's equation can be used to damp plasma waves in a nondrifting case, but leads to instability when $ku_0 > \omega_p$ in the drifting case. Suppose that the particle advance is described by Eq. (2) with $c_s = 0$ for $s \geqslant 1$ and that Gauss' law is represented by

$$\frac{\partial}{\partial x}[(1-\varepsilon)\,E_n + \varepsilon E_{n-1}] = \rho_n, \tag{B.3}$$

where ρ_n is the charge density, and ε is a centering parameter satisifying $0 \leqslant \varepsilon \leqslant 1$.

This alters the relation between the Fourier amplitudes of the linearized displacement and acceleration, and, hence, modifies the dispersion relation

$$X/A\Delta t^2 = -(1 - \varepsilon + \varepsilon z^{-1} e^{ik u_0 \Delta t})/\omega_p^2 \Delta t^2 = c_0 + z/(z-1)^2, \tag{B.4}$$

where z depends on the Doppler-shifted frequency.

For $u_0 = 0$, the stability condition arising from Eq. (B.4) is

$$c_0 + ((1 - 2\varepsilon)/\omega_p^2 \Delta t^2) > \tfrac{1}{4}. \tag{B.5}$$

To ensure stability at all values of $(\omega_p \Delta t)^2$ for a given value of c_0, it is required that $\varepsilon < \frac{1}{2}$. With the identifications $c_1 = \varepsilon/\omega_p^2 \Delta t^2$ and $c_0' = c_0 + (1 - \varepsilon)/\omega_p^2 \Delta t^2$, Fig. 1 provides details on the stability and damping characteristics of the plasma oscillations.

For finite u_0, Eq. (B.4) is equivalent to

$$\begin{aligned}(1 - \varepsilon) \sin^2(\theta/2) \\ = (\omega_p \Delta t/2)^2 \, [1 - 4c_0 \sin^2(\theta/2) - 4(\varepsilon/\omega_p^2 \Delta t^2) \sin^2(\theta/2) \, e^{i\omega \Delta t}].\end{aligned} \tag{B.6}$$

In the limit $\omega_p \Delta t \ll 1$, $k u_0 \Delta t \ll 1$, Eq. (B.6) has solutions

$$\omega = k u_0 \pm \omega_p [1 - (c_0 \omega_p^2 \Delta t^2/2(1 - \varepsilon)) - i\varepsilon((k u_0 \pm \omega_p) \Delta t/2(1 - \varepsilon))]. \tag{B.7}$$

The fast wave is damped, and for $k u_0 > \omega_p$ the slow wave is destabilized. The damping and growth rates are proportional to the time step Δt.

The stability of the fast and slow space-charge waves using the differencing scheme based on Eq. (2) is due to having introduced the dissipation into particle equations that are invariant under Galilean transformation. Attempting to introduce dissipation by biasing the time-centering of a Eulerian field equation, as in Eq. (B.3), leads to instability because such a modification destroys Galilean invariance. An interpretation of the stability and damping characteristics can be given in terms of a frequency-dependent, complex-valued plasma conductivity [12].

ACKNOWLEDGMENTS

It is a pleasure to acknowledge conversations with J. Denavit, R. Mason, D. Forslund, B. Godfrey, and J. Brackbill. This collaboration was a result of a workshop on implicit methods organized principally by C. K. Birdsall. This work was performed under the auspices of the U. S. Department of Energy, by the Lawrence Livermore National Laboratory under Contract W-7405-Eng-48.

REFERENCES

1. A. B. LANGDON, *J. Comput. Phys.* **30** (1979), 202.
2. A. FRIEDMAN, A. B. LANGDON, AND B. I. COHEN, *Comments Plasma Phys. Controlled Fusion* **6** (1981), 225.
3. J. DENAVIT, *J. Comput. Phys.* **42** (1981), 337.
4. R. J. MASON, *J. Comput. Phys.* **41** (1981), 233.
5. A. B. LANGDON, A. FRIEDMAN, AND B. I. COHEN, Implicit large-timestep particle simulation of plasmas, *J. Comput. Phys.*, submitted.
6. T. L. CRYSTAL, J. DENAVIT, AND C. E. RATHMANN, *Comments Plasma Phys. Controlled Fusion* **5** (1979), 17.
7. C. F. CURTISS AND J. O. HIRSCHFELDER, *Proc. Nat. Acad. Science. U.S.A.* **38** (1952), 235.
8. C. W. GEAR, "Numerical Initial Value Problems in Ordinary Differential Equations" p. 217, Prentice–Hall, Englewood Cliffs, N.J., 1971 (for $k = 2$).
9. O. BUNEMAN, *J. Comput. Phys.* **1** (1967), 517.
10. I. B. BERNSTEIN, *Phys. Rev.* **109** (1958), 10; T. KAMIMURA, T. WAGNER, AND J. M. DAWSON, *Phys. Fluids* **21** (1978), 115.
11. C. K. BIRDSALL, G. R. BREWER, AND A. V. HAEFF, *Proc. IRE* **41**, 865 (1953).
12. B. I. COHEN, "Effects of Numerical Dissipation on Simulation of Fast and Slow Space-Charge Waves," First Quarter Progress Report on Plasma Theory and Simulation, January 1–March 31, 1980, Electronics Research Laboratory, University of California, Berkeley, p. 20.